Tsunami Induced Scour Around Monopile Foundations

Larsen, Bjarke Eltard ; Fuhrman, David R.; Baykal, Cüneyt; Sumer, B. Mutlu

Published in:
Coastal Engineering

Link to article, DOI:
10.1016/j.coastaleng.2017.08.002

Publication date:
2017

Document Version
Peer reviewed version

Tsunami-induced scour around monopile foundations

Bjarke Eltard Larsen[a,*], David R. Fuhrman[a], Cneyt Baykal[b], B. Mutlu Sumer[c]

[a]*Technical University of Denmark, Department of Mechanical Engineering, Section of Fluid Mechanics, Coastal and Maritime Engineering, DK-2800 Kgs. Lyngby, Denmark*

[b]*Middle East Techincal University, Department of Civil Engineering, Ocean Engineering Research Center, Dumlupinar Blvd. 06800, Cankaya, Ankara, Turkey*

[c]*Technical University of Denmark, Department of Mechanical Engineering, Section of Fluid Mechanics, Coastal and Maritime Engineering, DK-2800 Kgs. Lyngby, Denmark. Present adress: BM Sumer Consultancy and Research, Istanbul Technical University, ARI Teknokent 3, B110, 34467, Maslak, Istanbul, Turkey*

Abstract

A fully-coupled (hydrodynamic and morphologic) numerical model is presented, and utilized for the simulation of tsunami-induced scour around a monopile structure, representative of those commonly utilized as offshore wind turbine foundations at moderate depths i.e. for depths less than 30 m. The model is based on solutions to Reynolds-averaged Navier-Stokes equations, coupled with two-equation $k-\omega$ turbulence closure, with additional bed and suspended load descriptions forming the basis for sea bed morphology. The model is first validated for flow, bed shear stresses, and scour within a steady current, where a generally excellent match with experimentally-based results is found. A methodology for maintaining and assessing hydrodynamic and morphologic similarity between field and (laboratory) model-scale tsunami events is then presented, combining diameter-based Froude number similarity with that based on the dimensionless wave boundary layer thickness-to-monopile diameter ratio. This methodology is utilized directly in the selection of governing tsunami wave parameters (i.e. velocity magnitude and period) used for subsequent simulation within the numerical model, with the tsunami-induced flow modelled as a long sinusoidally-varying current. The flow, sediment transport, and scour processes beneath up to ten tsunami waves are simulated in succession. These illustrate a generally accumulative scour process i.e. a relatively rapid scour induced by the leading wave, with an additional build-up of the scour depth during additional trailing waves. The resulting scour seems to approach an equilibrium value after sufficient time duration, which corresponds reasonably to that predicted by existing steady-current scour depth expression, afteraccounting for the finite boundary layer thickness induced by the unsteady tsunami wave, i.e. it is important to incorporate both current-like, as well as wave-like aspects of the long tsunami event. Based on the simulated results, a simple methodology for predicting the tsunami-induced scour depth in engineering practice is finally developed. This methodology is demonstrated to match the predicted scour development for all of the simulated flows considered, ranging from the series of transient tsunami waves to the steady-current limit.

Keywords: Tsunamis, Scour, Monopiles, Morphology, Computational Fluid Dynamics, Turbulence modelling

1. Introduction

Tsunamis are long waves, typically having periods the order of minutes to hours, that are generated by sudden motions of the sea bed e.g. due to undersea earthquakes or landslides. When such waves approach and/or reach the shoreline, they are potentially catastrophic, as has been well documented e.g. in the recent tsunami event that occurred in the Indian Ocean (2004), as well as in the Tohoku tsunami off the coast of Japan (2011).

While the run-up, inundation, and destructive potential of tsunami events has received considerable attention in the literature, the associated interaction with the sea bed i.e. boundary layer dynamics, induced sediment transport, and resultant sea bed morphology, have received relatively little specific attention. Such issues and processes are important, however, both in assessing potential larger scale deposition and erosion in affected coastal regions, as well as in understanding smaller scale erosion, such as tsunami-induced local scour around coastal and offshore structures (e.g. monopiles, piers, pipelines, and breakwaters), which can potentially contribute to their failure. Williams and Fuhrman (2016) simulated a series of tsunami-scale boundary layers, emphasizing that they may be both current-like due to their long durations, but also wave-like, in the sense that they are unsteady and that the boundary layer may not span the entire water depth. This assertion is likewise consisten with field measurements of Lacy et al. (2012). Studies investigating tsunami-induced scouring around coastal and offshore structures in any context are few, but include e.g. Wilson et al. (2012), who studied sediment scour and deposition within harbors; Chen et al. (2013), who studied tsunami-induced scour at coastal roadways; and Bricker et al. (2012), who conducted a field study of scour depths measured on the landward side of seawalls and floodwalls, as well as beside a building foundation footing, from the 2011 Tohoku tsunami. Experimental investigations on the tsunami-induced scour specifically around monopiles are seemingly limited to that of Tonkin et al. (2003), who studied the scour promoted by incident solitary waves

*Corresponding author
Email address: bjelt@mek.dtu.dk (Bjarke Eltard Larsen)

around a cylinder on a sloping beach, where the cylinder was mounted near the shoreline and to Nakamura et al. (2008) who studied scour around a square pile induced by solitary and long waves. The experiments by Tonkin et al. (2003) were also simulated numerically using a nonlinear shallow water model by Pan and Huang (2012), with the intent of simulating tsunami-induced scour around bridge piers. At this point it is worth emphasizing that studying tsunamis as solitary waves does not allow for their effective period and wave amplitude to be determined independently, and as a result the solitary wave duration is likely too short to represent geophysical tsunami events (see e.g. the discussion of Madsen et al. (2008)).

As seen from the above, most of the works considering the general topic of tsunami-induced scour have only recently been published i.e. in the past few years. Hence, a detailed understanding of the underlying processes, as well as general structure vulnerability, is presently lacking. The present study aims to further the understanding of tsunami-induced scour, by numerically investigating tsunami-induced flow and scour processes around a monopile structure, representative of those commonly utilized as offshore wind turbine foundations.

While the scour around monopiles due e.g. to waves and tidal currents has been extensively studied (see e.g. Sumer and Fredsøe (2002)), the potential scour around offshore wind turbine foundations induced by tsunami attack has not been previously studied, either experimentally or numerically. To ensure proper design, it is therefore important that a detailed understanding of the potential tsunami-induced scour around such structures be improved.

2. Hydrodynamic and turbulence model description

In this section the hydrodynamic model is presented. The flow is simulated by solving the incompressible Reynolds-averaged Navier-Stokes equations (RANS) and the continuity equation, coupled with a two-equation k-ω turbulence model for closure. The continuity equation and the RANS equations are, respectively, given in (1) and (2):

$$\frac{\partial u_i}{\partial x_i} = 0, \tag{1}$$

$$\frac{\partial u_i}{\partial t} + u_j \frac{\partial u_i}{\partial x_j} = -\frac{1}{\rho}\frac{\partial p}{\partial x_j} + \frac{\partial}{\partial x_j}\left(2\nu S_{ji} + \frac{\tau_{ij}}{\rho}\right), \tag{2}$$

where u_i are the mean components of the velocities, x_i are the Cartesian coordinates, p is the pressure, t is the time, S_{ij} is the mean strain rate tensor given by

$$S_{ij} = \frac{1}{2}\left(\frac{\partial u_i}{\partial x_j} + \frac{\partial u_j}{\partial x_i}\right), \tag{3}$$

and τ_{ij} is the Reynolds stress tensor, which is expressed according to the Boussinesq approximation

$$\tau_{ij} = -\overline{u_i' u_j'} = 2\nu_T S_{ij} - \frac{2}{3}k\delta_{ij}. \tag{4}$$

Here the overbar signifies time (ensemble) averaging, ν_T is the eddy viscosity, δ_{ij} is the Kronecker delta, and

$$k = \frac{1}{2}\overline{u_i' u_i'} \tag{5}$$

is the turbulent kinetic energy density. In the above a prime superscript denotes turbulent (fluctuating) velocity components.

To achieve closure, the k-ω turbulence model by Wilcox (2006, 2008) will be utilized. This model includes the following transport equations for the turbulent kinetic energy density k and the specific dissipation rate ω:

$$\frac{\partial k}{\partial t} + u_j \frac{\partial k}{\partial x_j} = \tau_{ij}\frac{u_i}{x_j} - \beta^* k\omega + \frac{\partial}{\partial x_j}\left[\left(\nu + \sigma^*\frac{k}{\omega}\right)\frac{\partial k}{\partial x_j}\right], \tag{6}$$

$$\frac{\partial \omega}{\partial t} + u_j \frac{\partial \omega}{\partial x_j} = \alpha\frac{\omega}{k}\tau_{ij}\frac{\partial u_i}{\partial x_j} - \beta\omega^2 + \frac{\sigma_d}{\omega}\frac{\partial k}{\partial x_j}\frac{\partial \omega}{\partial x_j} + \frac{\partial}{\partial x_j}\left[\left(\nu + \sigma\frac{k}{\omega}\right)\frac{\partial \omega}{\partial x_j}\right]. \tag{7}$$

The closure coefficients are given as $\alpha = 0.52$, $\beta = 0.078$, $\beta^* = 0.09$, $\sigma = 0.5$, $\sigma^* = 0.6$, $\sigma_{do} = 0.125$, and

$$\sigma_d = H\left(\frac{\partial k}{\partial x_j}\frac{\partial \omega}{\partial x_j}\right)\sigma_{do} \tag{8}$$

where $H(\cdot)$ is the Heaveside step function, which takes a value of unity if the argument is positive and zero otherwise.

In this model the eddy viscosity, which is present in the Reynolds stress tensor via the Boussinesq approximation, is given by

$$\nu_T = \frac{k}{\tilde{\omega}}, \tag{9}$$

with $\tilde{\omega}$ defined according to:

$$\tilde{\omega} = \max\left[\omega, C_{lim}\sqrt{\frac{2S_{ij}S_{ij}}{\beta^*}}\right], \tag{10}$$

where the second part of the expression is a stress limiting feature, with $C_{lim} = 7/8$.

The computational domain is discretized into finite volumes of quadrilateral blocks in varying shapes and dimensions. Figure 1 shows an example computational mesh typical of that used for the forthcoming scour simulations, which consist of two steady current validation simulations and two tsunami scour simulations. The computational domain, unless stated otherwise, has the following dimensions: length, $l = 20D$, width, $w = 15D$, and height, $h = 2D$, in which D is the monopile diameter. The total number of cells comprising the computational domains utilized is 170,496 with the near-bed cells having a height $O(d)$, in which d is the grain size. The monopile is located at the center of the domain $(x, y) = (0, 0)$. It is emphasized that considerable effort has been put into optimizing the computational mesh for convergence while at the same time keeping the computational time affordable. The length of $20D$ for the tsunami simulations is justifiable as is it sufficient to simulate steady current scour, which can be viewed as the infinite period limit for waves, see the forthcoming validation in Section 5.

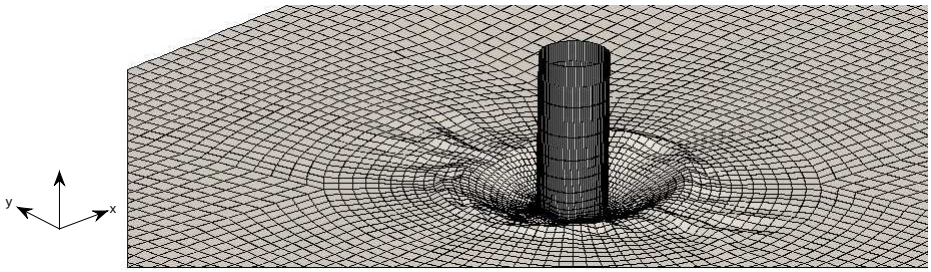

Figure 1: Example of the mesh in the vicinity of the monopile used in the scour simulations

2.1. Boundary conditions

The boundary conditions for the hydrodynamic model are as follows: The friction wall boundaries, that is the monopile and the seabed, will have a no-slip condition imposed such that velocities are zero. The top boundary will be modelled as a frictionless lid meaning that vertical velocities are set to zero, and horizontal velocities and scalar hydrodynamic quantities have zero vertical gradient. This means that the top boundary does not represent the free surface of tsunami waves and the simulations are performed as single-phase simulations. As described in Roulund et al. (2005) this is reasonable provided that the depth based Froude number Fr_h is sufficiently small. In the simulated tsunami cases $Fr_h = U_m/\sqrt{gh} \leq 0.2$, where U_m is the velocity magnitude beneath the tsunami waves. In the two steady current validation cases to be shown later $Fr = U/\sqrt{gh} = O(0.4)$ which is slightly larger, but not radically different, than O(0.2) where Roulund et al. (2005) showed that there was negligible free surface effect. Similar conditions were considered by Baykal et al. (2015). Therefore the flows considered will be fairly well represented in the lid simulations although some variations can occur in the two steady current cases such as the absence of a flow in the radial direction, caused, otherwise, by the head difference between the surface elevation in front and at the side edge of the monopile. It is emphasized that the two steady current cases are performed primarily to validate the model's ability to capture the isolated effect of the limited boundary layer thickness on the scour depth, which is ideally accomplished using the rigid lid.

The bottom and the monopile surface are modelled utilizing a generalized wall function approach. The friction velocity is determined from the tangential velocity at the nearest cell center, based on the profile of Cebeci and Chang (1978):

$$\frac{u}{U_f} = 2\int_0^{y_c^+} \frac{dy^+}{1+\left[1+4\kappa^2(y^+ + \Delta y_{cc}^+)^2 C\right]^{1/2}}, \tag{11}$$

$$C = [1-\exp(-(y^+ + \Delta y_{cc}^+)/25)]^2, \tag{12}$$

$$\Delta y_{cc}^+ = 0.9\left[\sqrt{k_s^+} - k_s^+ \exp\left(-\frac{k_s^+}{6}\right)\right], \tag{13}$$

who generalized the van Driest van Driest (1956) profile to incorporate potential roughness effects, with $y_c = \Delta y/2$ being the normal distance from the wall to the cell center, where Δy is the thickness of the near wall cell, $k_s = 2.5d$ is Nikuradse's equivalent sand roughness and $y_c^+ = y_c U_f/\nu$. The boundary conditions for k and ω are then as described by Fuhrman et al. (2014)

$$\frac{k}{U_f^2} = \min\left\{A\Delta y_c^{+2}, \frac{1}{\sqrt{\beta^*}}\right\}, \tag{14}$$

$$\frac{\omega\nu}{U_f^2} = \max\left\{\frac{B}{\Delta y_c^{+2}}, \frac{1}{\sqrt{\beta^*}\kappa\Delta y_c^+}\right\}. \tag{15}$$

The first arguments in these functions ensure that these variables follow their proper scaling $k \sim y^2$ and $\omega \sim 1/y^2$ for near wall cells within the viscous sub-layer (see e.g. Wilcox (2006)). The values $A = 1/(\delta^{+2}\sqrt{\beta^*}) = 0.02466$ and $B = \delta^+/(\sqrt{\beta^*}\kappa) = 96.885$ are utilized, which ensure a continuous transition to the (fully-turbulent) second arguments at $\Delta y_c^+ = \delta^+$, where $\delta^+ = 11.626$ is taken as the viscous sub-layer thickness (in dimensionless wall coordinates). At the bottom and the monopile surface the eddy viscosity is not calculated from (9), but is instead calculated from

$$U_f^2 = \frac{\tau_b}{\rho} = (\nu + \nu_T)\frac{dU}{dz}. \tag{16}$$

Following Larsen et al. (2016), the flow is driven by a Dirichlet condition i.e. the velocity is specified at the left-hand inlet boundary, which comes from a separate one-dimensional vertical (1DV) pure boundary layer simulation, made utilizing the same model as described above. In this boundary layer simulation the flow is driven by a body force which will be specified in the description of the simulated cases. From here the velocity profile, as well as the profiles for k and ω, are sampled and utilized as inlet boundary conditions within the scour simulations. Through this approach the special characteristics of the tsunami boundary layer are incorporated directly within the driving inlet flow.

3. Sediment transport and morphological models

In this section the sediment transport and morphological models are described. The description will only include the most essential details since the implementation of the models have already been described and discussed by Jacobsen (2011), as well as in the recent publication of Jacobsen et al. (2014).

The model for the bed load transport corresponds to that of Roulund et al. (2005), who extended the model of Engelund and Fredsøe (1976) to also include three dimensional effects as well as bed slope modifications to the Shields parameter.

The suspended load is calculated by solving the advection-diffusion equation for the concentration (see *e.g.* Fredsøe and Deigaard, 1992, p. 238):

$$\frac{\partial c}{\partial t} + (u_j - w_s\delta_{j3})\frac{\partial c}{\partial x_j} = \frac{\partial}{\partial x_j}\left[(\nu + \beta_s\nu_T)\frac{\partial c}{\partial x_j}\right], \qquad (17)$$

where c is the suspended sediment concentration, w_s is the settling velocity, and $\beta_s = 1$ is utilized meaning that the sediment diffusivity takes the same value as the eddy viscosity. The settling velocity is calculated by the approach given in Fredsøe and Deigaard (1992), which is based on the drag coefficient of the falling sediment grains.

Equation (17) is solved on a sub-set of the main computational mesh where the near-bed cells below a given reference level b are removed. At this reference level a reference concentration, c_b, boundary condition is imposed. There are several formulations of c_b but here the one by Engelund and Fredsøe (1976) is utilized. The concentration at the reference level is given by

$$c_b(\theta) = \frac{c_0}{(1 + 1/\lambda_b)^3}, \qquad (18)$$

in which $c_0 = 0.6$ is the maximum value for the concentration, and the linear concentration λ_b is

$$\lambda_b^2 = \frac{\kappa^2\alpha_1^2}{0.013s\theta}\left(\theta - \theta_c - \frac{\pi}{6}\mu_d p_{EF}\right), \qquad (19)$$

where

$$p_{EF} = \left[1 + \left(\frac{\pi\mu_d}{6(\theta - \theta_c)}\right)^4\right]^{-\frac{1}{4}} \qquad (20)$$

and

$$\theta = \frac{\tau_b}{\rho g(s-1)d} = \frac{U_f^2}{(s-1)gd} \qquad (21)$$

is the Shields parameter. Throughout the present work the coefficient of dynamic friction is set to $\mu_d = 0.51$ and the critical Shields parameter θ_c is computed from a base value $\theta_{c0} = 0.05$, accounting for bed-slope effects as in Roulund et al. (2005).

Following Fuhrman et al. (2014), a reference level of $b = \alpha_1 d = 3.5d$ is utilized. This is quite similar to the value $b = 3.6d$ utilized by Liang and Cheng (2005). To prevent un-physical "overloading" conditions i.e. where the concentration just above the bed exceeds c_b calculated from the reference concentration formula, the solution suggested by Justesen et al. (1986) is invoked. That is, if the concentration close to the bed exceeds the reference concentration, the value is in practice taken from the cell adjacent to the boundary. At the top and monopile boundaries a zero-flux condition for c is utilized.

3.1. Morphological model

The morphological updating routine is based on the sediment continuity (Exner) equation

$$\frac{\partial h}{\partial t} = \frac{1}{1-n}\left[-\frac{\partial q_{Bi}}{\partial x_i} + D + E\right], \qquad i = 1, 2 \qquad (22)$$

where $n = 0.4$ is the bed porosity and

$$D = (w_s - u_3)c_b, \qquad E = (\nu + \beta_s\nu_T)\frac{\partial c}{\partial x_3}\bigg|_{x_3=b} \qquad (23)$$

are the deposition and erosion coming from the suspended sediment model. The Exner equation is based on instantaneous sediment transport fields and therefore the morphological and hydrodynamic times are equivalent. To ensure that the bed slopes do not exceed the angle of repose the sand slide model described in detail by Roulund et al. (2005) is implemented. In the present work, this model is activated at positions where the local bed angle exceeds the angle of repose $\phi_s = 32°$, and is de-activated once the local bed angle has been reduced to 31.9°.

The equations comprising the fully-coupled model outlined above are solved numerically using the open-source CFD toolbox OpenFOAM®, version 1.6-ext, making use of a finite volume spatial discretization with a collocated variable arrangement, in conjunction with a standard PIMPLE algorithm. Again, for further details see Jacobsen et al. (2014). The fully-coupled model presented above has also been utilized recently by Baykal et al. (2015) who simulated the current-induced scour process around a vertical monopile cylinder, by Baykal et al. (2017) who simulated scour and backfilling around piles in waves as well as by Fuhrman et al. (2014), Larsen et al. (2016) and Bayraktar et al. (2016) in the simulation of wave-induced and wave-plus-current-induced scour and/or backfilling processes beneath submarine pipelines.

4. Re-analysis of existing research

Before proceeding with validation of the model, some of existing research on scour around monopiles will first be revisited, with particular focus on the effects of a finite boundary layer thickness, which turns out to be highly important to the understanding of tsunami-induced scour processes around offshore monopiles. The reason for this is two-fold. First, while data exists, there is not currently available a closed-form expression for predicting the equilibrium scour depth accounting for the finite boundary layer thickness. Second, the existing formula for the time scale of the scour development, will give rise to some extremely small time scales when extrapolating to full scale. Therefore the experimental data is revisited and a new expression for the time scale is proposed.

According to Sumer and Fredsøe (2002) and Melville and Sutherland (1988) the non dimensional equilibrium scour depth, S_e/D is a function of θ, the sediment gradiation, the boundary layer thickness to pile size ratio δ/D, the sediment to pile-size ratio, the shape factor and the alignment factor. For the present simulations, with uniform sediment distribution and a circular pile, however the scour depth becomes only a function of θ and δ/D. If the situation is in the live-bed regime the influence of θ is rather small, and effectively the scour depth is primarily a function of δ/D. In Figure 2 experimental data compiled by Melville and Sutherland (1988) (also reproduced in Sumer and Fredsøe (2002)) is shown together with a new line

representing the following expression

$$\frac{S_e}{S_0} = 1 - \exp\left(-0.9\frac{\delta}{D}\right), \tag{24}$$

where $S_0/D = 1.3$ is the widely-accepted equilibrium current induced scour value around a circular pile (without depth limitation), see Sumer and Fredsøe (2002). This expression is a fit to the data which will be used later in estimating equilibrium scour depths. Included in the figure are also results involving steady current scour from the present study as well as one result from the numerical study (using the same model) by Baykal et al. (2015). These results will be compared and discussed in forthcoming sections. It can be seen that equation

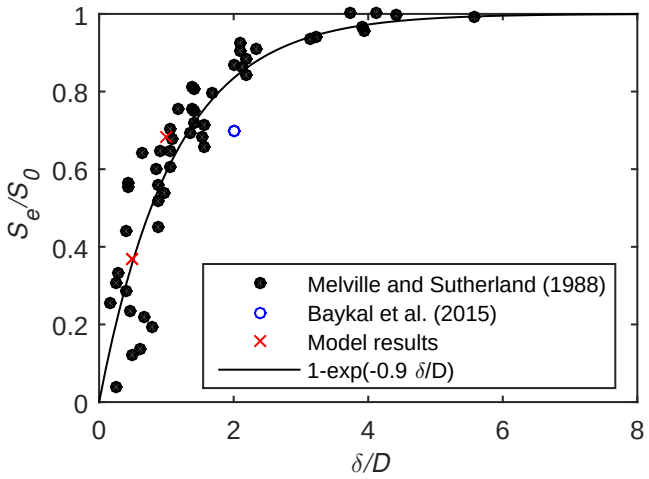

Figure 2: Effect of boundary layer thickness on equilibrium scour depth. Experimental results compiled by Melville and Sutherland (1988) (also reproduced by Sumer and Fredsøe (2002))

(24) gives a quite good approximation to the experimental results even though the experiments show some scatter (the standard deviation on S_e/S_0 from the expression is 0.11). There is a tendency for smaller scour depths as the boundary layer thickness to pile diameter reduces. The reason for this is that the decreased boundary layer thickness in turn decreases the size of the horseshoe vortex and thus reduces the scouring capacity.

Based on a series of steady current scour experiments, Sumer et al. (1992b) likewise proposed the following regression equation for estimating the scour time scale:

$$T_s^* = \frac{\sqrt{g(s-1)d^3}}{D^2} T_s = \frac{1}{2000}\frac{\delta}{D}\theta^{-2.2}, \tag{25}$$

which can be interpreted as the time it takes for significant scour to occur. Here T_s is the dimensional time scale and T_s^* is the non-dimensional time scale. It is important to emphasize, however, that (25) is based on experiments spanning the parametric range $0.039 \leq \delta/D \leq 10$ and $0.062 \leq \theta \leq 0.29$. Care must therefore be taken when extrapolating this expression to field conditions e.g. where Shields parameters $\theta = O(1)$ may be reached, see Table 2 and 3 in section 6. Based on a re-investigation of the experimental data set of Sumer et al. (1992b), we propose a slightly modified expression:

$$T_s^* = \frac{1}{400}\left(\frac{\delta}{D}\right)^{0.7}\theta^{-1.5}. \tag{26}$$

The fit of the original experimental data set to both expressions (25) and (26) is shown in Figure 3. Included in the figure

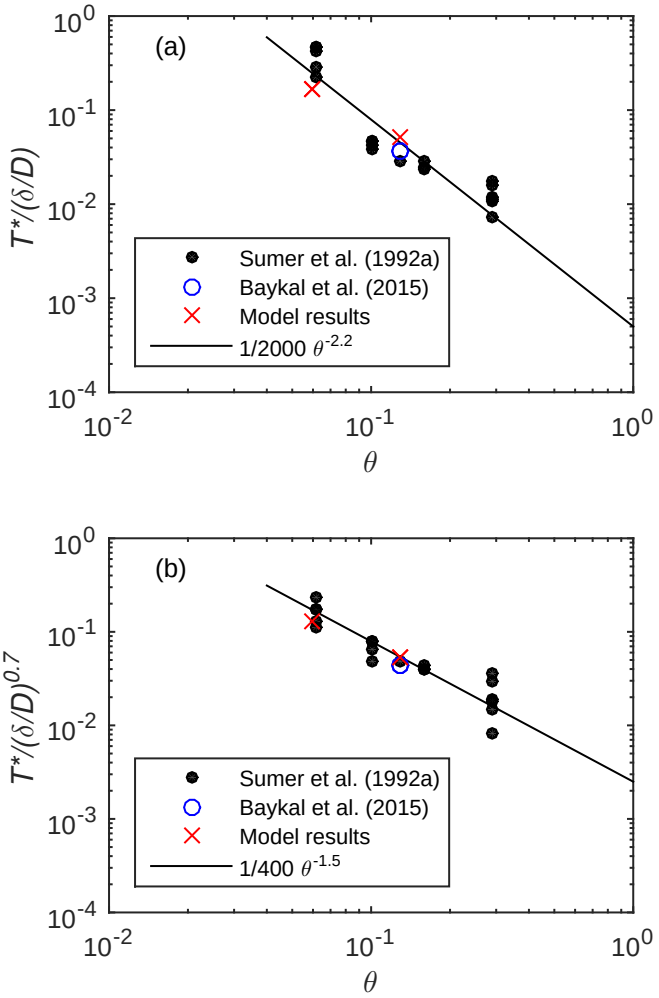

Figure 3: Comparison of two regression equations: (a) (25) and (b) (26) for predicting the time scale of scour, based on the experimental data set of Sumer et al. (1992b) .

are also the two time scales calculated from the forthcoming simulations. From this figure it is seen that the new expression (26), shown in Figure 3b, slightly improves clustering of the data compared to the original expression (25), shown in Figure 3a, though both expressions yield similar time scale predictions within the parametric range of the data. Due to the lower magnitude exponent on the Shields parameter θ, i.e. power -1.5 rather than -2.2, it is felt that the modified expression (26) will be less prone to extrapolation errors at field scales. The reduced power of θ also makes sense on the following physical grounds. The time scale of the scour process should be proportional to the volume of the scour hole, $\mathcal{V} \propto D^3$, divided by the product of sediment transport rate, q_T, and width of the scour hole $\propto D$:

$$T_s \propto \frac{\mathcal{V}}{q_T D} \propto \frac{D^3}{q_T D} = \frac{D^2}{q_T}. \tag{27}$$

Inserting this into the expression for the non-dimensional time scale (25) gives

$$T_s^* = \frac{\sqrt{g(s-1)d^3}}{D^2} T_s \propto \frac{\sqrt{g(s-1)d^3}}{q_T} = \Phi_T^{-1} \propto \theta^{-3/2} \quad (28)$$

where Φ_T is the non-dimensional transport rate and is assumed to scale as $\theta^{3/2}$, common to many sediment transport formulae, see e.g. Fredsøe and Deigaard (1992). Based on these considerations, the scour time scale will therefore be estimated from the modified expression (26) in what follows.

5. Model validation

In this section, the numerical model described above will be validated for scour around a vertical cylindrical pile mounted on a horizontal plane soil bed, subjected to a steady current. Given the generally long periods (spanning several minutes to hours) typical of tsunamis, validation based on steady current flows can be considered more relevant than e.g. based on experiments using typical wind wave scales. Given the large computational costs of advanced CFD models such as those utilized in the present paper, simulations are necessarily limited to laboratory spatial and temporal scales. This model has already been used to simulate both detailed flow structures, bed shear stresses as well as scour around a wall mounted monopile by Baykal et al. (2015) and it has therefore been partly validated for the purpose of this study. In addition two more steady scour cases are simulated here to further validate the models ability to correctly capture the relationship between S_e/D and δ/D, as well as the temporal scour development and thus the time scale of the scour process. In table 1 the setup of the two additional cases is given where the boundary layer height δ is taken as the

Table 1: Set-up of the two additional validation cases with d=0.17 mm and D=0.1 m.

Test	δ (m)	U (m/s)	U_f (cm/s)	δ/D	θ	Fr
1	0.05	0.246	1.28	0.5	0.06	0.35
2	0.10	0.430	1.89	1.0	0.13	0.43

flow depth. The flow will be driven via the inlet by prescribing the horizontal velocity u, the turbulent kinetic energy density k, and the specific dissipation rate ω. As described in Section 3 the profiles for the three quantities comes from a separate 1DV simulation which is driven by a body force given by

$$F = \frac{U_f^2}{\delta} \quad (29)$$

where U_f is chosen to give the desired Shields parameter.

In Figure 4 the computed non-dimensional scour depth is plotted as a function of non-dimensional time. Included in the plots (dashed lines) is also the well known expression for the temporal development of the scour process as given by Sumer and Fredsøe (2002)

$$\frac{S}{D} = \frac{S_e}{D}\left(1 - \exp\left(-\frac{t^*}{T_s^*}\right)\right) \quad (30)$$

where t^* is the non-dimensional time given by

$$t^* = \frac{\sqrt{g(s-1)d^3}}{D^2} t. \quad (31)$$

The non-dimensional time scale has been calculated by equation (26) and the equilibrium scour depth by equation (24), both of which are experimentally based. As expected it can be seen that an initial phase of extensive scouring is followed by a longer phase of limited scouring, slowly approaching the equilibrium scour depth. The scour process of the two cases follows equation (30) quite well, although in both cases the initial scour phase in the model is a bit more rapid. The simulated and predicted equilibrium scour depths in both cases are quite similar, especially recalling the scatter from Figures 2 and 3. That the

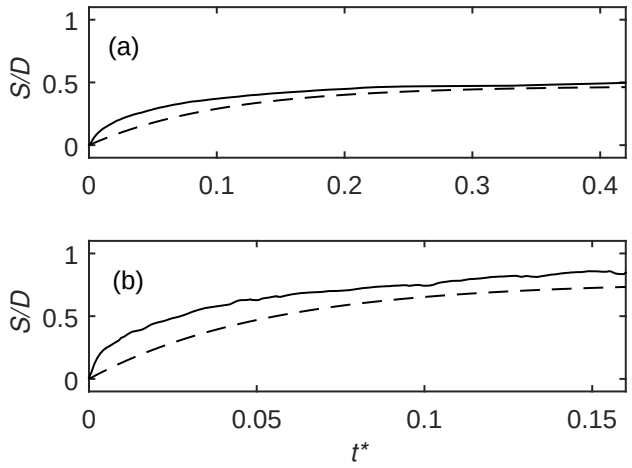

Figure 4: Computed temporal evolution of the scour depth under steady current conditions (full lines) of a) Test 1 and b) Test 2. Also shown (dashed lines) is that from (30) after invoking (24) and (26).

equilibrium scour depth is predicted well by the model can also be seen by re-inspection of Figure 2. Here it can be seen that model successfully captures the reduced scour depths due to the finite boundary layer thickness. The model also captures the time scale of the scour process which can be seen by inspection of Figure 3. Here the modelled time scales are compared with the experimental as well as equation (26). The modelled time scales are calculated by integrating the scour curve according to

$$T_s^* = \int_0^{t^*_{max}} \frac{S_{max} - S}{S_{max}} dt^*, \quad (32)$$

where S_{max} is the maximum scour depth at any given time and t^*_{max} is the time at which the maximum scour occurs.

In Figure 5 the equilibrium bed profile, in the near-pile region, from Test 2 is shown. Here some of the characteristic features of the steady current scour around a monopile can be seen. Upstream of the monopile the expected semi-circular shape of the scour hole with bed slopes equal to the angle of repose is clearly visible, whereas the slope downstream of the monopile is more gentle and the shape of the hole cannot be characterized as semi-circular. Further, downstream of the monopile bed material is deposited along the edges of the scour hole as a result of

small-scale counter-rotating stream-wise phase-averaged vortices close to the bed and further downstream deposited material moves towards the center forming a bar as a result of large-scale counter-rotating streamwise phase-averaged vortices, as discussed in detail by Baykal et al. (2015) see their Figure 12a and by Petersen (2014). It can also be seen that the surrounding

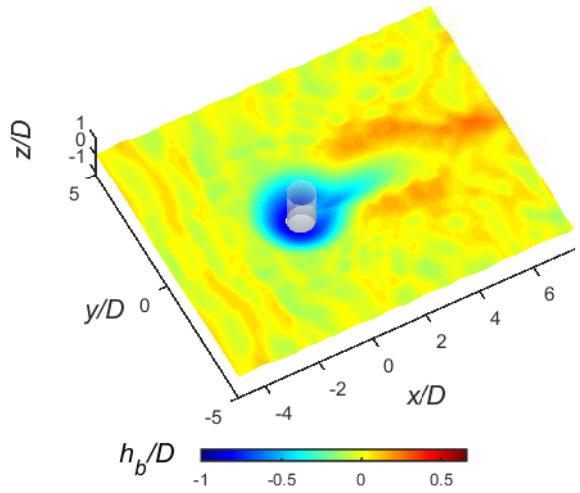

Figure 5: Equilibrium near-pile bed profile of Test 2

bed contains ripples. At full field scales, sheet flow conditions may in fact be reached and hence, the small scale ripple features developing in the present (model scale) result may in fact be related to scale effects. The presence of the ripples do not seem to influence the scour process, as no ripples are present in the neighbourhood of the pile where the flow field is disturbed and ripple formation prevented.

6. Similarity of tsunami field and model scales

As noted in the previous section, due to the large computational expenses associated with advanced CFD models, it is presently only feasible to simulate such scour processes around a monopile at model (laboratory) spatial and temporal scales. The reason for this is that while much of the mesh might follow a standard length scaling, the near bed mesh does not, as the utilized model and field scale grain sizes are very similar. This would of course increase the needed number of cells but more importantly the the small nearbed cells combined with much higher full scale velocities would require the time step to be substantially smaller to ensure typical Courant number based restrictions. Therefore, prior to conducting such numerical simulations involving tsunami-induced scour, it is necessary to first establish a methodology for maintaining similarity of model and full field scales, in terms of properly chosen dimensionless quantities. In this section such a methodology for establishing hydrodynamic and morphodynamic similarity within an unsteady tsunami-induced scouring process will be introduced and described. This methodology will then be utilized to determine parameters used for numerical simulation at model scales in the subsequent section.

As inspiration for obtaining typical full tsunami scales, we will now consider a well-known measurement of the 2004 Indian Ocean tsunami event from the yacht Mercator, taken at a water depth h=14 m, which is depicted in Figure 6. Based

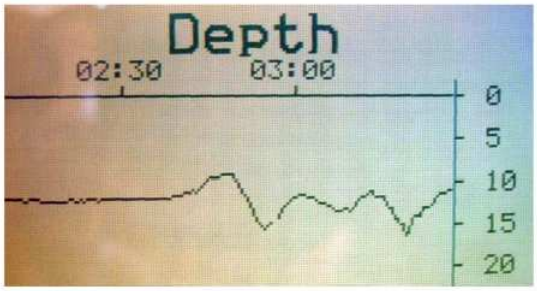

Figure 6: Sound-meter registration of the Indian Ocean tsunami on December 26, 2004 from the yacht Mercator in the bay of Nai Ham, at the southwestern tip of Phuket, Thailand. The vertical axis measures depth in meters (from the keel i.e. 2 m below mean water level); The horizontal axis measures time in hours. Source Thomas Siffer (www.thomassiffer.be).

on this signal, Madsen and Fuhrman (2008) estimated that the leading wave of this tsunami could be reasonably represented as sinusoidal, with a wave period T=13 min and surface elevation amplitude A=2.5 m. Based on these parameters, the velocity magnitude U_m beneath such an event can be readily estimated, as a first approximation, based on linear shallow water theory

$$U_m = A\sqrt{\frac{g}{h}} \tag{33}$$

yielding U_m=2.1 m/s. This follows a similar methodology as also utilized in the tsunami-scale boundary layer simulations of Williams and Fuhrman (2016). It can be noted that a sinusoidal description for this tsunami event can be considered a much closer approximation than would e.g. a signal based on a solitary wave description, which would only include positive surface displacement, and which would not allow for the effective period and wave amplitude to be determined independently (see e.g. the discussion of Madsen et al. (2008)). Note also that, based on records of free surface fluctuations at several locations during the 2011 Japan Tohoku tsunami, Chan and Liu (2012) have likewise concluded that the leading tsunami waves, in both near-field and far field regions, can be characterized as small amplitude long waves i.e. consistent with the linear shallow water description utilized above. The previously mentioned velocity magnitude U_m and period T will be utilized in what follows as characteristic values, representative of tsunamis at full scale, though obviously precise values may differ from these for other specific events and/or locations. Note that the corresponding water depth (h=14 m) for this signal is conveniently appropriate for the present considerations, as monopile foundations are commonly utilized within offshore wind turbines out to depths no larger than about 30 m. Additionally, for the purposes of our discussion, a full-scale monopile diameter of D=5 m will be considered, which is typical for offshore wind turbine foundations. Finally, for the sake of our discussion, bed sediments at full scale will be considered to have a typical grain

size d=0.30 mm i.e. corresponding to medium-fine sand.

Based on the values above, the following important hydrodynamic quantities can be estimated using widely-utilized dimensionally-correct expressions from the literature. The wave boundary layer thickness δ can be estimated based e.g. on the well-known expression of Fredsøe and Deigaard (1992)

$$\frac{\delta}{D} = \frac{k_s}{D} 0.09 \left(\frac{a}{k_s} \right)^{0.82} \tag{34}$$

where $k_s = 2.5d = 0.75$ mm and $a = U_m T/(2\pi) = 261$ m is the amplitude of the free stream orbital motion. Utilizing these yields the estimate δ=2.36 m for the parameters considered. The value has additionally been confirmed from tsunami-scale boundary layer simulations by Williams and Fuhrman (2016), which is based on the one-dimension vertical turbulent boundary layer model of Fuhrman et al. (2013). Notice that, though expectedly much larger than typical wind wave boundary layer thicknesses of up to say 10 cm, the estimated boundary layer thickness is still only a fraction of the water depth, h=14 m, in this example. The depth-based Froude number $Fr_h = U_m/(gh)^{0.5}$=0.18 is also relatively small (< 0.2). Hence, for the conditions considered, the effects associated with the physical water depth h can be considered small, with associated length scales then based entirely on the monopile diameter D. Accordingly, we define a dimensionless Froude number as follows:

$$Fr_D = \frac{U_m}{\sqrt{gD}} \tag{35}$$

As discussed previously, due to their generally long periods, it is expected that the instantaneous flow and resulting scour process around a monopile during a tsunami event will more closely resemble those under steady flow conditions, rather than those beneath wind waves. Therefore, to achieve hydrodynamic similarity we will select the flow parameters U_m and T such that we maintain similarity in terms of the diameter-based Froude number (35), as well as the boundary layer thickness-to-diameter ratio δ/D, based on (34). Equating the Froude number (35) ensures that the adverse pressure gradient induced by the presence of the structure itself will be similar at both model and field scales, i.e. that the ratio of the excess stagnation pressure head in front of the monopile $U_m^2/(2g)$-to-pile diameter D will be maintained. Similarly, by maintaining similarity in δ/D, we ensure that the relative size of the horseshoe vortex, which is expected to largely govern the scouring process, will be similar at both model and full scales. Also of interest, is the so-called Keulegan-Carpenter number

$$KC = \frac{U_m T}{D} \tag{36}$$

which governs the formation and relative extension of the wake pattern in oscillatory motion. Additionally, it is likewise of interest to estimate the time scale of the expected scour process. Under both current and wave conditions, this is widely known to depend on the Shields parameter. For waves this can be defined as

$$\theta_m = \frac{U_{fm}^2}{(s-1)gd}, \tag{37}$$

where the maximum value of the friction velocity U_{fm} can be estimated from

$$U_{fm} = \sqrt{\frac{f_w}{2}} U_m, \tag{38}$$

where the rough-bed wave friction factor f_w expression from Fuhrman et al. (2013) is utilized

$$f_w = \exp\left(5.5 \left(\frac{a}{k_s} \right)^{-0.16} - 6.7 \right). \tag{39}$$

This is likewise consistent with the general findings of Williams and Fuhrman (2016), who found that this expression maintained reasonable accuracy, even when extrapolated to full tsunami-scale. With an estimation of the Shields parameter the time scale of scour T_s can now be estimated. Due to the long durations typical of tsunamis, this time scale will be based on existing steady current scour research, equation (26), but invoking the expected tsunami-induced wave boundary layer thickness from (34). Hence, both current-like and wave-like features of tsunami-induced flows will be accounted for. In a similar fashion the equilibrium scour depth can be estimated by invoking the same boundary layer thickness in equation (24), again utilizing $S_0 = 1.3$

Choosing a scaling factor of $\lambda = 50$ and maintaining similarity in terms of the Froude number as well as the boundary layer thickness to pile diameter ratio results in a model scale wave period T=52.9 s, and a velocity magnitude U_m=0.297 m/s. It can be noted that, consistent with the notion that tsunamis are much longer than wind waves, the resulting period is significantly longer than those typically used in model-scale scour experiments involving wind waves, which would typically involve periods $T = O(1$ s).

The resulting values, based on the presently described parameterization, are summarized in Table 2, under the full scale column. Both dimensional, as well as dimensionless, quantities are tabulated. Importantly, it can now be ascertained that the full scale tsunami period-to-scour time scale ratio $T/T_s = 0.54 = O(1)$ i.e. typical tsunami periods can be expected to be the same order of magnitude as expected scour time scales. This is an important recognition, and implies that the scouring process induced by tsunami events may, or may not, be of sufficient duration to reach equilibrium scour conditions. Either scenario seems realistic, as equilibrium scour conditions can require several scour time scales to be reached.

The resulting dimensional and dimensionless parameters based on the discussed model scale are likewise summarized in Table 2, where the sediment grain diameter d=0.17 mm utilized in the previously discussed model validation is maintained. The dimensionless quantities maintained at both full and model scales are highlighted in bold. The methodology described herein is designed to yield hydrodynamic similarity at model and full scales. However, as can be seen from Table 2, it does not yield precise similarity in all other dimensionless parameters. As is well-known, the Reynolds number is

Table 2: Case 1: Comparison of resulting dimensional (above horizontal line) and dimensionless (below horizontal line) quantities at selected field and simulated model conditions. Dimensionless quantities maintained at both scales are highlighted in bold.

	Full scale	Model scale
D	5 m	0.1 m
d	0.3 mm	0.17mm
T	13 min = 780 s	52.9 s
U_m	2.1 m/s	0.297 m/s
U_f	0.0745 m/s	0.0146 m/s
δ	2.36 m	0.047 m
T_s	1449 s	76.4 s
S	2.25 m	0.045 m
s	2.65	2.65
$\mathbf{Fr_D}$	**0.30**	**0.30**
$\delta/\mathbf{D}$	**0.47**	**0.47**
KC	328	157
$Re_D = U_m D/\nu$	10^7	$3 \cdot 10^4$
θ_m	1.1	0.078
T/T_s	0.54	0.69
S/D	0.45	0.45

Table 3: Case 2: Comparison of resulting dimensional (above horizontal line) and dimensionless (below horizontal line) quantities at selected field and simulated model conditions. Dimensionless quantities maintained at both scales are highlighted in bold.

	Full scale	Model scale
D	2.5 m	0.1 m
d	0.3 mm	0.17mm
T	13 min = 780 s	87.2 s
U_m	2.1 m/s	0.42 m/s
U_f	0.0745 m/s	0.0190 m/s
δ	2.36 m	0.094 m
T_s	589 s	57 s
S	1.86 m	0.074 m
s	2.65	2.65
$\mathbf{Fr_D}$	**0.42**	**0.42**
$\delta/\mathbf{D}$	**0.94**	**0.94**
KC	655	366
$Re_D = U_m D/\nu$	$5.3 \cdot 10^6$	$4.2 \cdot 10^4$
θ_m	1.1	0.13
T/T_s	1.33	1.53
S/D	0.74	0.74

obviously not maintained, though this is not expected to greatly influence the scour process, as the Reynolds number does not play an important role in the formation of the horseshoe vortex. Additionally, e.g. the expected Shields parameter at model scale is an order of magnitude below that expected at full scale. Both are above critical, however, hence both conditions can be considered as effectively in the live bed scour regime which is necessary for scour similarity, see e.g Figure 3.24 in Sumer and Fredsøe (2002). These differences are also accounted for, at least in part, in the dimensionless period-to-scour time scale ratio T/T_s, which while not identical (0.54 versus 0.69), is quite close at both full and model scales. Hence, the morphological process occurring over an individual wave period at model scale will represent a similar portion of the scour process as expected at full scale. This case will be denoted Case 1.

In addition to the case just described, to extend the parametric range considered one more case will likewise be simulated. Here the full scale monopile is assumed to have half the diameter, i.e. $D = 2.5$ m (in this case the scaling factor is $\lambda = 25$ such that the mesh can conveniently be reused). The full scale and model scale quantities, calculated utilizing the same similarity approach, for this case are similarly summarized in table 3. Note that in this case $\delta/D = 0.94$, nearly double that of Case 1. This will be denoted Case 2.

7. Simulation of tsunami-induced scour

Based on the preceding section, we will now simulate the tsunami-induced scour process around a monopile using the previously described and validated fully-coupled CFD numerical model. The idealized flow induced by our prototypical tsunami event will be introduced via the inlet (left hand) boundary by prescribing the horizontal velocity u, the turbulent kinetic energy density k, and the specific dissipation rate ω. The profiles for the three quantities comes from a separate 1DV simulations which were driven by a body force given by

$$F = U_m \frac{2\pi}{T} \cos\left(\frac{2\pi}{T} t\right). \tag{40}$$

For the purposes of our numerical model experiment, the model scale parameters presented previously in Tables 2 and 3 (i.e. U_m=0.297 m/s and T=52.9 s as well as U_m=0.42 m/s and T=87.2 s) will be utilized to drive the simulations. For Case 1 ten and Case 2 four, full tsunami periods will be simulated in succession. The motivation for considering multiple periods is four-fold: First, a real-life tsunami may well consist of a leading wave, in addition to several trailing waves; Second, consideration of the successive periods will shed light on tsunami-induced scour in the presence of pre-existing scour holes; Third, this will increase the effective total scour time, and hence can be considered relevant e.g. for other tsunami events having longer period than those specifically being considered herein; Fourth, it will shed light on whether the our understanding of the physical process, and therefore also our estimation of the equilibrium scour depth, is correct. As an indication of computational time for the present simulations, each successive model-scale period requires approximately 10 days of CPU time, when simulated in parallel on eight modern processors i.e. the full simulations require up to approximately four months to complete.

The simulated time series of the scour depth for Case 1, taken at both the front and back face of the monopile, are first presented in Figure 7. It is seen from Figure 7 that the first half-cycle (flow going rightward) expectedly produces significant scour at the front (left) side, which is then followed by a similar scouring process on the back (right) side during the second half-cycle (flow going leftward). These scouring processes can be mainly attributed to separate horseshoe vortices forming on opposite sides during the two successive half cycles. This

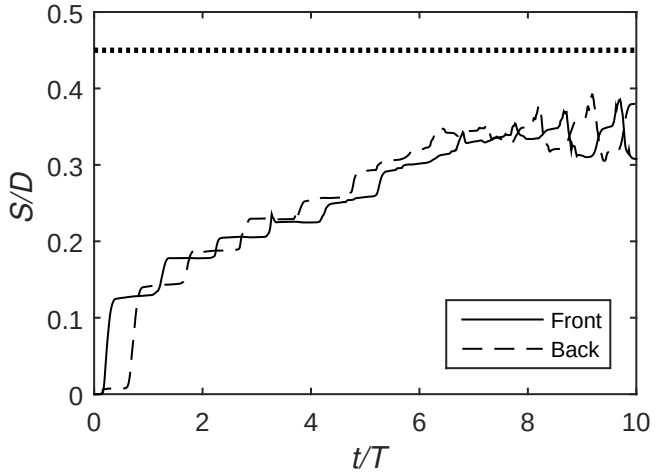

Figure 7: Computed time series of scour depth at the front and back face of the monopile for Case 1. The horizontal dashed line represents the equilibrium scour depth estimated from (24).

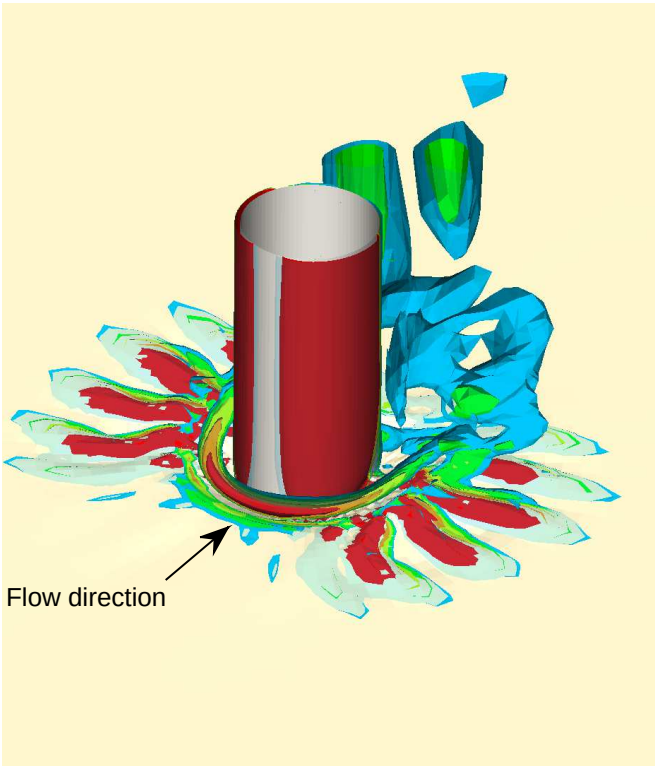

Figure 8: 3D view of instantaneous vortical structures around the monopile at t=1.25 T and a threshold of $Q = 2$ s^{-2}.

is illustrated in Figure 8 where instantaneous coherent vortical structures, identified by the so-called Q-criterion, around the monopile is depicted. The Q-criterion was originally formulated by Hunt et al. (1988) and is defined as

$$Q = \frac{1}{2}\left(\left|\Omega_{ij}\right|^2 - \left|S_{ij}\right|^2\right) > \Pi_E \tag{41}$$

where $\Omega_{ij} = 1/2(\partial u_i/\partial x_j - \partial u_j/\partial x_i)$ is the mean rotation tensor and Π_E is a threshold used to define eddy containing zones. In Figure 8 a horseshoe vortex is clearly seen in front of the monopile and further down stream the lee-wake vortices are clearly visible. This confirms the previous explaination, that the instantaneous flow and scour processes beneath a tsunami can be taken as resembling a current, but with finite boundary layer thickness limited by the growth duration. It may be noted that the Q-criterion has been extensively used in conjunction with scour and backfilling around piles in waves by Baykal et al. (2017)

Due to the relatively long times involved, the processes occurring during the two half cycles of the tsunami seem to be largely independent of one another. It should be noted that, in the present scenario, the first half-cycle may be taken as either representing a leading elevation or leading depression tsunami wave, depending on the orientation adopted. Beyond the first period, it is seen that the scour deepens at both front and back sides during the successive wave periods in a loosely stepwise fashion i.e. the observed scour process can be characterized as largely cumulative. In the final periods some backfilling is observed each time the flow reverses. This is interpreted as the scour hole finally being so large that most of the sand being removed from one side of the monopile cannot escape the hole but instead is being deposited at the other side of the monopile. As a reference value, the equilibrium scour depth predicted by (24), after invoking (34), yields $S_e/D = 0.45$. This value is also depicted in Figure 7 as the horizontal dashed line. As seen, after several periods of accumulation the resulting scour on both sides of the monopile seems to be gradually approaching this equilibrium value. Note that the relatively moderate equilibrium scour (at least in dimensionless terms i.e. $S_e/D < 0.5$) predicted in the present case, is again due to the finite boundary layer thickness-to-diameter ratio $\delta/D = 0.47$, which limits the relative size of the formed horseshoe vortices. Invoking the full scale monopile diameter D=5 m, however, this still correspond to considerable scour i.e. up to approximately $S = 2.25$ m for the full scale conditions considered. Based on the cumulative nature of the present results, it is reasonable to expect that the scour around a monopile will continue to build over the duration of a given tsunami event, ceasing when equilibrium scour depths are reached, which will occur only if the event is sufficiently long. Additionally, the effects on the scour associated with finite boundary layer thickness seem to be reasonably accounted for by the steady current expression (24), after invoking the tsunami wave boundary layer thickness from (34).

In Figure 9 the time series of the scour depth, taken at both the front and the back face of the monopile, for the Case 2 (corresponding to a full scale diameter of $D = 2.5$ m) is shown. The development of the scour depth in this case is similar to that of Case 1 in that the first half-cycle produces significant scour at the front side and the second produces significant scour at the back side. Further, beyond the first period the scour hole deepends in a stepwise cumulative fashion, and the depth is gradually approaching the equilibrium value calculated by invoking the boundary layer thickness in (24). The present case however exhibits one feature quite different from Case 1. Already in the first period, after the flow reversal sediment is being

transported from the back-side, backfilling into the front-side of the monopile. This process is then repeated when the flow re-reverses. This can be explained by the expected period to time scale ratio of this case being substantially larger than in Case 1, and thus within a half period there is sufficient time to transport substantial sediment all the way from one side of the monopile to the other.

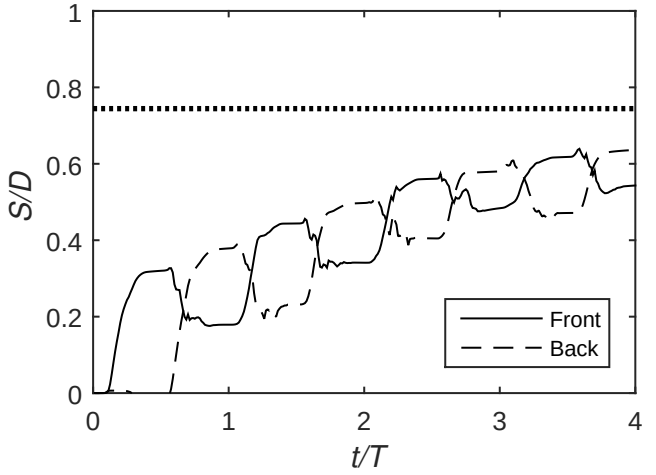

Figure 9: Computed time series of scour depth at the front and back face of the monopile for Case 2. The horizontal dashed line represents the equilibrium scour depth estimated from (24).

Snapshots of the computed scour holes at selected times when the flow is leftward ($t = 0.4T$, $1.4T$, and $2.4T$) as well as rightward ($t = 0.9T$, $1.9T$, and $2.9T$) are additionally depicted in Figures 10 (Case 1) and 11 (Case 2). These figures likewise illustrate the generally stepwise buildup of scour on the two opposing sides of the monopile during each successive half-cycle of the simulated tsunami (see again Figure 7). In addition to the scour occurring on the front and back faces of the monopile, small scale ripple-like features are also seen develop. For Case 1 the ripples appear first to the transverse sides of the monopile, and then alternatively to the front and back of the monopile as time progresses, and they are more pronounced than in Case 2. Such features tend to initially form during the flow reversal, due to settling of suspended sediments. For Case 2 the bed profile has more current-like features than Case 1. This can be explained by the period to time-scale ratio being larger in the slim diameter case, and thus each period represents a larger portion of the scouring process towards equilibrium.

The computed scour profiles along the model centerline (y=0), taken at the same instances as depicted in Figures 10 and 11, are similarly depicted in Figures 12 (Case 1) and 13 (Case 2). To ease comparison, these have been divided into times when the flow is leftward (Figure 12a and 13a, corresponding to the left-hand subplots of Figure 10 and 11) and rightward (Figure 12b and 13b, corresponding to the right-hand subplots on Figure 10 and 11). Inspection of the scour profiles, as a whole, demonstrates that reasonable symmetry is maintained throughout the scour process, consistent with the symmetric nature of the idealized (sinusoidal) flow description utilized. The asymmetry observed at any particular time is primarily due to the directionality of the flow (i.e. rightward or leftward directed) just experienced.

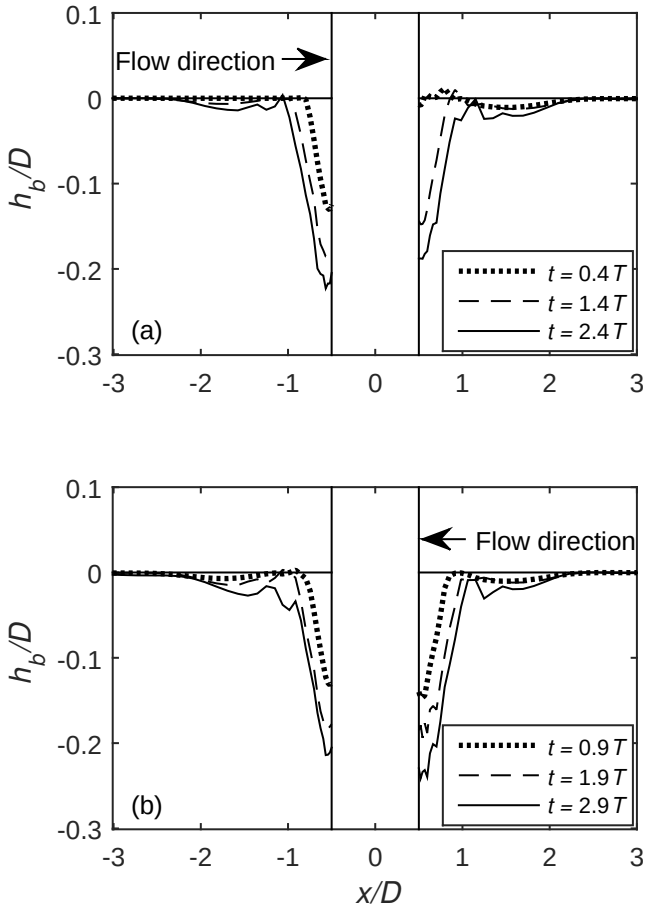

Figure 12: Computed scour profiles along the centerline for Case 1 for three consecutive periods

Based on the present results, in real (less idealized) tsunami events the asymmetry of the scour profile can be expected to depend strongly on the asymmetric nature of individual tsunami waves, which can of course vary widely from event to event. Considering the present results at half- and full-period intervals should provide a reasonable first indication regarding expected scour asymmetry, however.

8. Practical model for predicting tsunami-induced scour

As it is not always feasible in practice to perform advanced fully-coupled CFD simulations of tsunami-induced scour processes (even at model scales), especially for a large number of scenarios, it is of major importance that simpler methods be developed for predicting the tsunami-induced scour around monopile foundations in engineering practice. Such a simple practical method will be developed in the present section, which will utilize existing physical scour process knowledge, while also incorporating additional insight gained from the numerical simulation of the scour process presented in Section 7.

To begin making a practical assessment on the expected tsunami-induced scour around a monopile foundation, it is

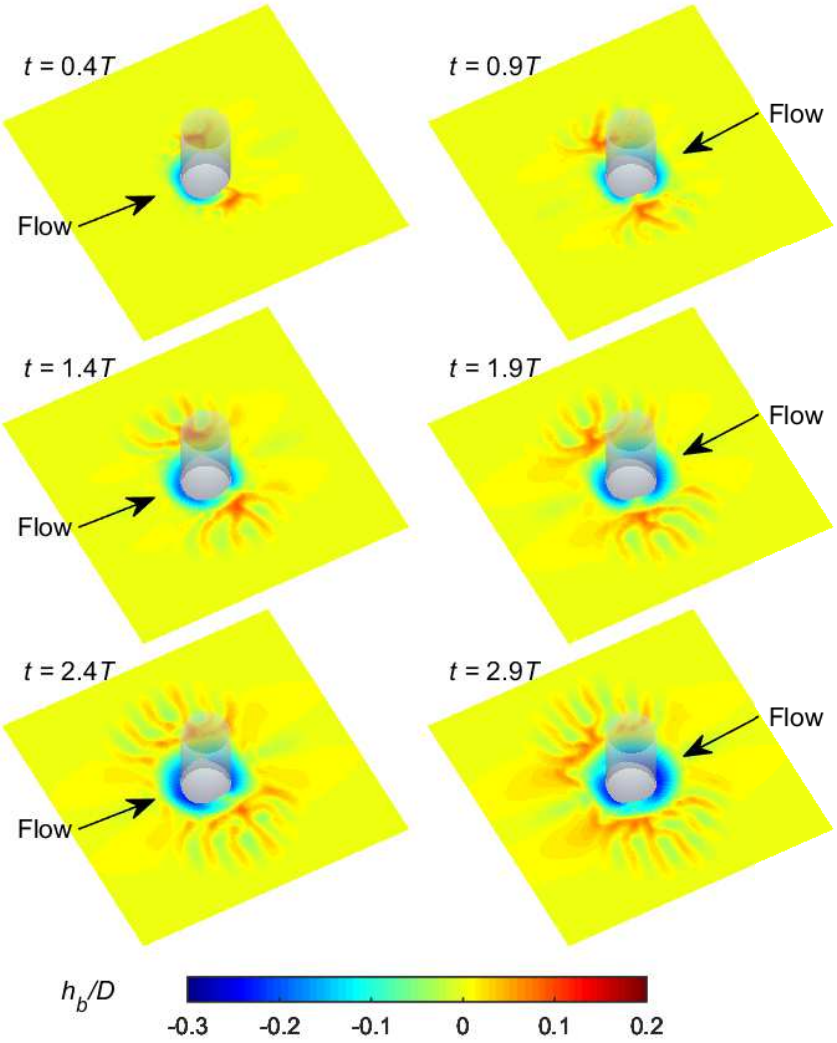

Figure 10: Bed profiles around the monopile for Case 1 for three different periods.

convenient to first estimate the maximum expected equilibrium scour that would be expected to occur at infinite time i.e. if a given tsunami event was repeated indefinitely. Taking into account the effect of a (potentially finite) boundary layer thickness-to-pile diameter ratio δ/D, this equilibrium scour S_e can be reasonably estimated according to (24) where the tsunami wave boundary layer thickness δ can be estimated directly from (34), and where the maximum potential current-induced scour (for large boundary layer thickness) may be taken as

$$\frac{S_0}{D} = 1.3 \pm \sigma_{S/D} \tag{42}$$

Here $\sigma_{S/D} = 0.7$ is the standard deviation of expected scour, as presented by Sumer et al. (1992a), which can be accounted for in practice to adjust for a desired level of conservativeness. In what follows, we aim to predict the mean expected scour, hence this standard deviation will be neglected i.e. we simply utilize $S_0/D = 1.3$ in (24). Now, as emphasized previously, typical tsunami periods can be expected to be the same order of magnitude as expected scour times scales. This, again, implies that true equilibrium scour depths may, or may not, be reached, depending on the duration of a given tsunami event, since reaching equilibrium can require several scour time scales. It is therefore important to take the expected time development of the scour process into account when making tsunami-induced scour predictions. Utilizing a scour time scale T_s estimated from (26), this temporal variation can then be described according to the following expression

$$\frac{S}{D} = \frac{S_e}{D}\left(1 - \exp\left(-\frac{t_s}{T_s}\right)\right), \quad t_s = n\psi T. \tag{43}$$

This resembles (30), which is commonly used to characterize typical time development of scour processes. In the equation above t_s represents the effective scour time, and n represents the integer number of successive waves characterizing a given tsunami i.e. n=1 can be utilized to predict the maximum scour

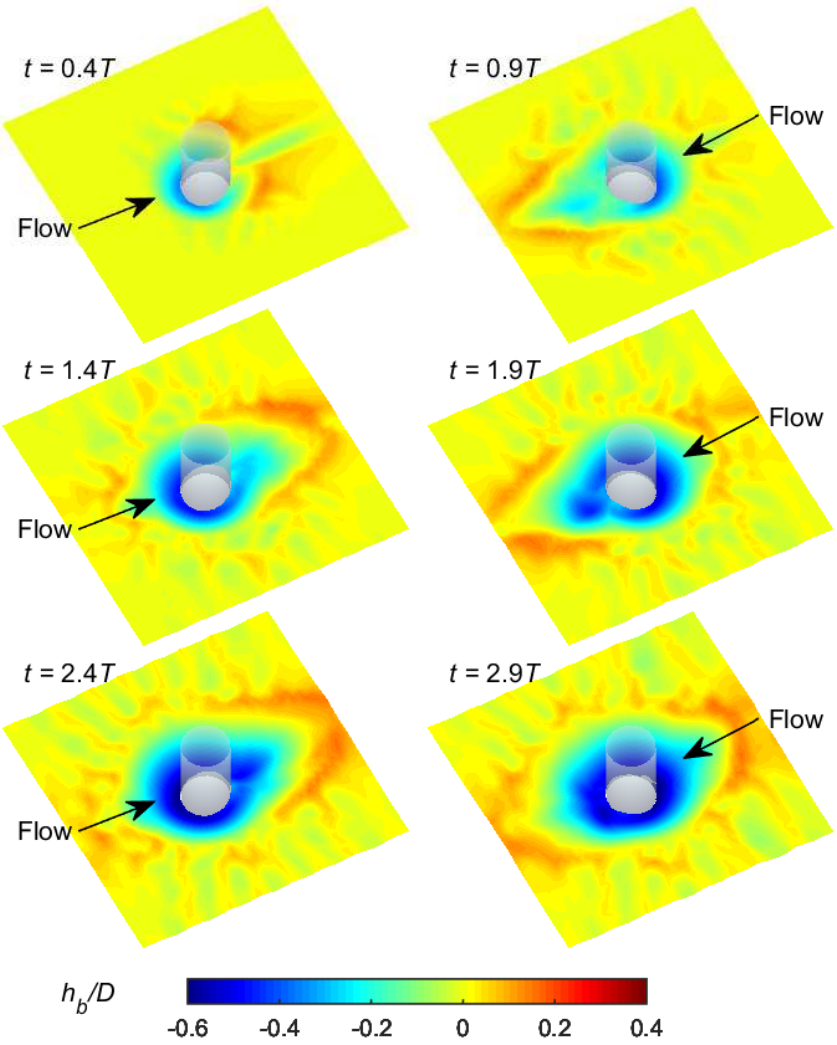

Figure 11: Bed profiles around the monopile for Case 2 for three different periods.

occurring during the leading tsunami wave, with n=2,3,... utilized for predicting the accumulated scour induced by any successive waves. The additional factor $\psi \leq 1$ can be taken to represent the effective scouring fraction of a period. Based on the stepwise fashion in which the scour hole deepens and the relative independence of the two half cycles, it is expected to be at least $\psi < 1/2$ (if a sinusoidal tsunami description is utilized as herein). In fact it can be expected to be somewhat lower than $1/2$ since θ is not at a maximum throughout the entire period. Therefore a value of $\psi = 1/3$ has been chosen for use in what follows as it is in line with the previous arguments and is seen to match the simulations well. Note that for large t_s, (43) will simply lead to equilibrium scour i.e. $S = S_e$.

To test the validity of the simple practical model described above, the predicted scour from the practical approach leading to (43) will be compared directly with the numerical scour results presented in Section 7. In Figures 14 and 15 the simulated scour process is shown together with scour curves obtained utilizing equations (43) invoking the tsunami boundary layer thickness for the calculation of S_e and T_s. Included in the figure is also the steady current estimate obtained by invoking the flow depth as the boundary layer thickness and setting $\psi = 1$. As can be seen, the simple predictive model proposed above does a consistently good job of predicting the scour observed within the numerical simulations, as it follows quite well the maximum scour depth within each period. The estimate is not exact, but recalling the scatter in the experimental results, leading to equation (24) on which the engineering model is built, the estimate is satisfactory. As expected the steady current estimate is somewhat higher, especially for Case 1, and this illustrates the importance of invoking the expected effect of the limited tsunami boundary layer thickness. It is emphasized that the approach proposed above is conveniently founded upon existing experimentally-based expressions for use in steady current scour, but invoking the boundary layer thickness and Shields parameter expected from tsunami wave events i.e. it effec-

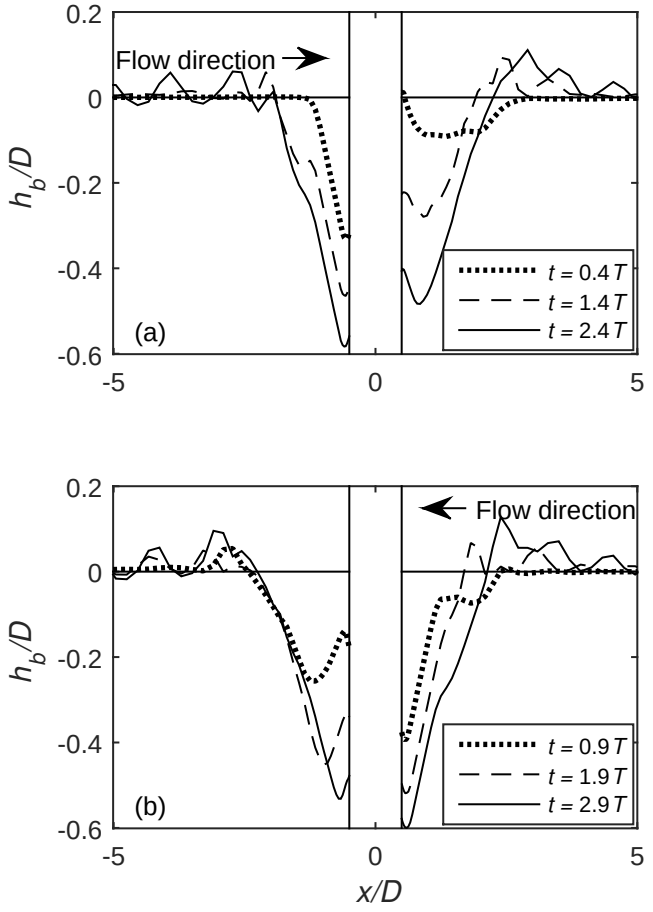

Figure 13: Computed scour profiles along the centerline for Case 2 for three consecutive periods

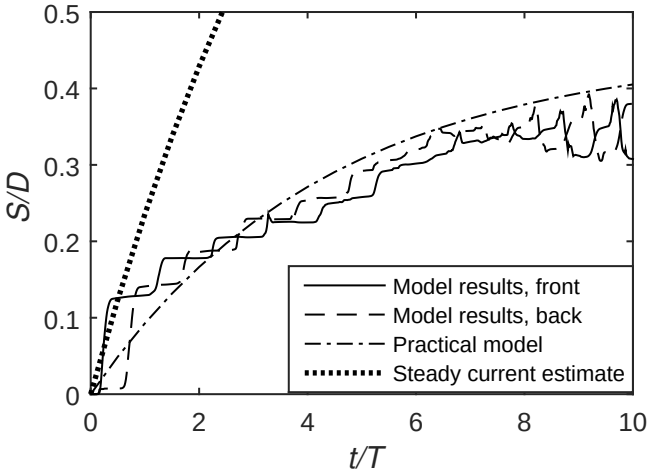

Figure 14: Comparison between the predicted and simulated scour depths for Case 1.

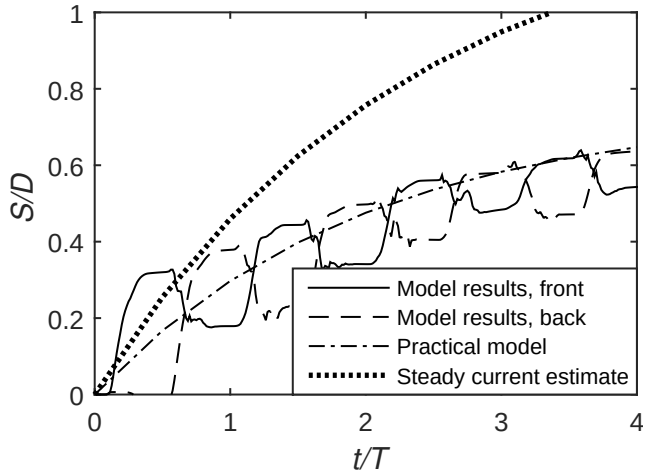

Figure 15: Comparison between the predicted and simulated scour depths for Case 2.

tively combines both current-like and wave-like properties of tsunamis. As such, at the infinite period limit, the practical model proposed is fully consistent with existing methodology for predicting equilibrium scour under steady current conditions. It is finally important to emphasize that the steady current limit can be considered quite physically relevant for scenarios involving tsunami-induced scour in some circumstances, at least as an upper bound. In particular, this limit would seem particularly relevant for tsunamis having very long duration (i.e. large T/T_s), for scour occurring at shallower water depths (where the boundary layer thickness δ can be taken as equivalent to the water depth h), or for tsunami-induced scour around smaller monopile diameters (i.e. where the boundary layer thickness-to-pile diameter ratio becomes large i.e. $\delta/D > 4$) e.g. those more typical of bridge piers.

To further highlight the predictive capability of the simple model, accumulated scour results from each of the successive wave periods in the simulations (see Figure 7 and 9) will be considered separately, with the results corresponding to the maximum scour occurring during a given period of interest. Results at both the front and back face of the monopile will be considered separately, for completeness. A plot summarizing the computed versus predicted (utilizing the present simple practical approach) maximum scour is depicted in Figure 16. For completeness the computed and predicted equilibrium value for the simulated current-induced scour Section 5, previously considered as model validation, is also shown (×) in Figure 16, as is the steady current result from Baykal et al. (2015) which again was simulated utilizing the same model. As can be seen, the simple predictive model proposed above does a consistently good job of predicting the scour observed within the numerical simulations, with all results resonably near the line of perfect agreement (full line) in Figure 16. This conclusion holds for the full range of flows considered: For the transient tsunami cases, though the simple model cannot predict all details, such as the momentary lee-side backfilling episodes observed on the front face, it adequately predicts the accumulative maximum scour occurring over all successive simulated tsunami periods. As discussed previously, relatively moderate S/D values are found for the tsunami scenarios considered, owing to effects associated with the finite boundary layer thickness, which seem to be properly accounted for. Such effects become less important at the steady current limit, leading to the larger S/D, which is also

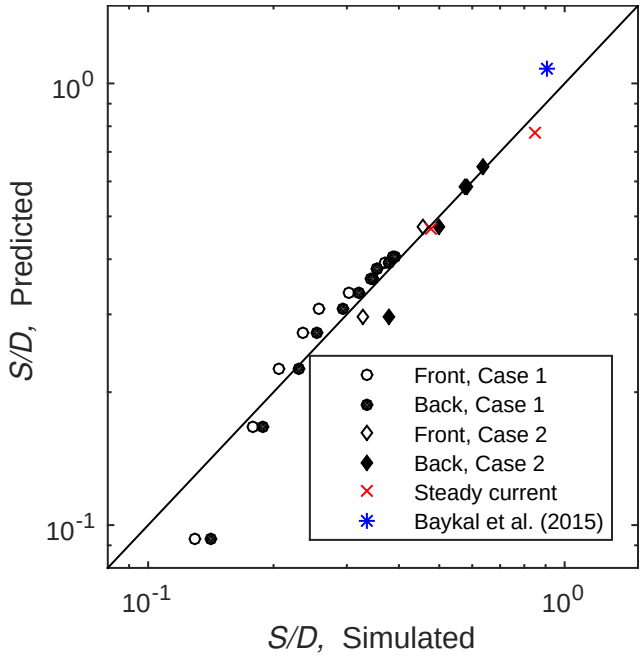

Figure 16: Comparison between the predicted and simulated scour depths.

adequately captured by the proposed simple approach.

9. Conclusions

This paper presents a numerical assessment for tsunami-induced scour around a monopile structure, as commonly utilized in practice as offshore wind turbine foundations. The basis of the numerical model is the advanced fully-coupled hydrodynamic and morphological CFD model presented in Jacobsen et al. (2014), and utilized specifically for simulating scour processes by Baykal et al. (2015), Fuhrman et al. (2014) and Larsen et al. (2016). The model hydrodynamics are based on Reynolds-averaged Navier-Stokes (RANS) equations, coupled with two-equation $k-\omega$ turbulence closure. These are then coupled with both bed and suspended sediment transport descriptions, which drive resultant morphology of the sea bed. Simulations of the scour process in steady current has been performed as model validation, complementing previous validation made by Baykal et al. (2015).

Due to computational expense, it is only feasible at present to simulate scour processes at model (laboratory) spatial and temporal scales. Therefore, prior to making any simulations, a methodology has been developed for establishing similarity (based on dimensionless numbers) between full tsunami and model scales, in precisely the same fashion as in hydraulic scale model experiments in which similarity is established between full scale real life and the hydraulic scale model. This methodology is based on a diameter-based Froude number, coupled with the dimensionless ratio of the expected boundary layer thickness-to-monopile diameter δ/D. The Froude similarity ensures similarity in the adverse pressure gradients induced by the presence of the structure itself, whereas the δ/D similarity ensures equivalent relative size of the horseshoe vortex in front of the monopile. Reasonable morphologic similarity of the scour process is also maintained, by ensuring that the dimensionless tsunami period-to-scour time scale ratios are similar. It is demonstrated that typical tsunami periods can be expected to be the same order of magnitude as expected scour time scales in real life. This implies that equilibrium scour conditions may, or may not, be reached, depending on the total duration of a given tsunami event.

Taking a well-known tsunami measurement from the 2004 Indian Ocean tsunami as a typical event at full scale (in terms of its surface amplitude and approximate period), input parameters are found based on the similarity principles described above. These are then utilized within simulations of the tsunami-induced scour process around a monopile foundation. The results generally demonstrate that, consistent with physical expectations due to their long periods, the tsunami-induced scour process reasonably resembles that under steady current conditions. Unlike steady current scour, however, the tsunami-induced scour process, under the conditions considered, can be limited by finite wave boundary layer thickness, rather than the flow depth. Hence, it is important to take into account both the current-like (due to their long periods), as well as their wave-like (unsteady) properties, to fully understand and assess the tsunami-induced scour process. This is consistent with the findings of tsunami-scale wave boundary layer simulations of Williams and Fuhrman (2016).

Based on existing scour knowledge, combined with the insight gained from the advanced CFD simulations, a simple methodology has been developed for predicting tsunami-induced scour around monopiles in practice. The method takes into account the time variation of the scour process as well as finite boundary layer thickness effect, and can hence be applied to predict the cumulative tsunami-induced scour under successive periods i.e. it is not limited to simply a leading wave description. The practical method makes modified use of existing experimentally-based expressions for predicting steady current scour and time scales, and hence is fully-consistent with these at this (infinite period) limit. The practical method is demonstrated to accurately predict all of the simulated scour depths considered in the present paper i.e. ranging from the simulated transient tsunami events to those induced by steady current flows.

10. Acknowledgements

The authors acknowledge support from the European Union project ASTARTE–Assessment, Strategy And Risk Reduction for Tsunamis in Europe, Grant no. 603839 (FP7-ENV-2013.6.4-3). The third and fourth author additionally acknowledges Innovative Multi-purpose Offshore Platforms: Planning, Design and Operation (MERMAID), 20122016, Grant Agreement No. 288710 of European Commission, 7th Framework Programme for Research.

References

Baykal, C., Sumer, B. M., Fuhrman, D. R., Jacobsen, N. G., Fredsøe, J., 2015. Numerical investigation of flow and scour around a vertical circular cylinder. Phil. Trans. Roy. Soc. A 373, article no. 20140104.

Baykal, C., Sumer, B. M., Fuhrman, D. R., Jacobsen, N. G., Fredsøe, J., 2017. Numerical simulation of scour and backfilling processes around a circular pile in waves. Coast. Eng. 122, 87–107.

Bayraktar, D., Ahmad, J., Eltard Larsen, B., Carstensen, S., Fuhrman, D. R., 2016. Experimental and numerical study of wave-induced backfilling beneath submarine pipelines. Coast. Eng. 118, 63–75.

Bricker, J. D., Francis, M., Nakayama, A., 2012. Scour depths near coastal structures due to the 2011 tohoku tsunami. J. Hydraul. Res. 50 (6), 637–641.

Cebeci, T., Chang, K. C., 1978. Calculation of incompressible rough-wall boundary-layer flows. AIAA J. 16, 730–735.

Chan, I.-C., Liu, P. L. F., 2012. On the runup of long waves on a plane beach. J. Geophys. Res. - Oceans 117 (8), 1–17.

Chen, J., Huang, Z., Jiang, C., Deng, B., Long, Y., 2013. Tsunami-induced scour at coastal roadways: a laboratory study. Natural Hazards 69 (1), 655–674.

Engelund, F., Fredsøe, J., 1976. A sediment transport model for straight alluvial channels. Nordic Hydrology 7, 293–306.

Fredsøe, J., Deigaard, R., 1992. Mechanics of Coastal Sediment Transport. World Scientific, Singapore.

Fuhrman, D. R., Baykal, C., Sumer, B. M., Jacobsen, N. G., Fredsoe, J., 2014. Numerical simulation of wave-induced scour and backfilling processes beneath submarine pipelines. Coast. Eng. 94, 10–22.

Fuhrman, D. R., Schløer, S., Sterner, J., 2013. RANS-based simulation of turbulent wave boundary layer and sheet-flow sediment transport processes. Coast. Eng. 73, 151–166.

Hunt, J. C. R., Wray, A. A., Moin, P., 1988. Eddies, streams, and convergence zones in turbulent flows. Center for Turbulence Research, Proceedings of the Summer Program.

Jacobsen, N. G., 2011. A full hydro- and morphodynamic description of breaker bar development. Ph.D. thesis, Technical University of Denmark, Kgs. Lyngby.

Jacobsen, N. G., Fredsøe, J., Jensen, J. H., 2014. Formation and development of a breaker bar under regular waves. Part 1: Model description and hydrodynamics. Coast. Eng. 88, 182–193.

Justesen, P., Fredsøe, J., Deigaard, R., 1986. The bottleneck problem for turbulence in relation to suspended sediment in the surf zone. In: Proc. 20th Int. Conf. on Coastal Engineering. pp. 1225–1239.

Lacy, J. R., Rubin, D. M., Buscombe, D., 2012. Currents, drag, and sediment transport induced by a tsunami. JOURNAL OF GEOPHYSICAL RESEARCH-OCEANS 117 (9), –.

Larsen, B. E., Fuhrman, D. R., Sumer, B. M., 2016. Simulation of wave-plus-current scour beneath submarine pipelines. J. Waterw. Port C-ASCE 142 (5), 08216001.

Liang, D., Cheng, L., 2005. Numerical model for wave-induced scour below a submarine pipeline. J. Waterw. Port C-ASCE 131, 193–202.

Madsen, P. A., Fuhrman, D. R., 2008. Run-up of tsunamis and long waves in terms of surf-similarity. Coast. Eng. 55, 209–223.

Madsen, P. A., Fuhrman, D. R., Schäffer, H. A., 2008. On the solitary wave paradigm for tsunamis. J. Geophys. Res. 113, article no. C12012.

Melville, B., Sutherland, A., 1988. Design method for local scour at bridge piers. J. Hydraul. Eng. ASCE 114 (10), 1210–1226.

Nakamura, T., Kuramitsu, Y., Mizutani, N., 2008. Tsunami scour around a square structure. Coastal Engineering Journal 50 (2), 209–246.

Pan, C., Huang, W., 2012. Numerical modeling of tsunami wave run-up and effects on sediment scour around a cylindrical pier. J. Eng. Mech. - ASCE 138 (10), 1224–1235.

Petersen, T. U., 2014. Scour around Offshore Wind Turbine Foundations. Ph.D. thesis, Technical University of Denmark. Department of Mechanical Engineering, Kgs. Lyngby, Denmark.

Roulund, A., Sumer, B. M., Fredsøe, J., Michelsen, J., 2005. Numerical and experimental investigation of flow and scour around a circular pile. J. Fluid Mech. 534, 351–401.

Sumer, B. M., Christiansen, N., Fredsøe, J., 1992a. Scour around a vertical pile in waves. J. Waterw. Port C-ASCE 118, 15–31.

Sumer, B. M., Christiansen, N., Fredsøe, J., 1992b. Time scale of scour around a vetical pile. In: Proc. of the Second International Offshore and Polar Engineering Conference. Vol. 3. pp. 308–315.

Sumer, B. M., Fredsøe, J., 2002. The Mechanics of Scour in the Marine Environment. World Scientific, Singapore.

Tonkin, S., Yeh, H., Kato, F., Sato, S., 2003. Tsunami scour around a cylinder. J. Fluid Mech. 496 (496), 165–192.

van Driest, E. R., 1956. On turbulent flow near a wall. J. Aeronautical Sciences 23, 1007–1011, 1036.

Wilcox, D. C., 2006. Turbulence Modeling for CFD, 3rd Edition. DCW Industries, Inc., La Canada, California.

Wilcox, D. C., 2008. Formulation of the k-ω turbulence model revisited. AIAA J. 46, 2823–2838.

Williams, I. A., Fuhrman, D. R., 2016. Numerical simulation of tsunami-scale wave boundary layers. Coast. Eng. 110, 17–31.

Wilson, R., Davenport, C., Jaffe, B., 2012. Sediment scour and deposition within harbors in california (usa), caused by the march 11, 2011 tohoku-oki tsunami. Sedimentary Geology 282, 228–240.